ACS OMEGA

Open Access

http://pubs.acs.org/journal/acsodf

Article

Synthesis and Characterization of N-Doped Seaweed Biochar and Removal of Cationic Dyes

Meiyuan Fu, Jia Xu, Tiantian Lu, Qianhui Ma, Yun Luo, Wen Feng, and Xianghui Wang*

Cite This: *ACS Omega* 2025, 10, 18753−18763

Read Online

ACCESS | Metrics & More | Article Recommendations

ABSTRACT: The development of functional porous carbon materials has attracted great attention in various fields. In this work, N-doped algal biochar (NABc) materials were successfully prepared by an impregnation and calcination methods using Dicyandiamide as a modifier. The specific surface area, average pore volume, and average pore diameter of NABc1%, were 693.92 $m^2 \cdot g^{-1}$, 0.162 $cm^3 \cdot g^{-1}$ and 6.76 nm, respectively. The high efficiency of NABc1% in adsorbing the cationic dyes rhodamine B and methylene blue from water may be attributed to the rich pore structure of NABc1%. The adsorption experiments show that the removal rates of rhodamine B and methylene blue by NABc1% in 90 min are 99.4 and 96.2%, respectively, which are obviously higher than those before modification. The experimental results of adsorption kinetics show that the adsorption process is more consistent with the quasi-second-order kinetic fitting equation (R^2 = 0.961, 0.998). The results of isothermal adsorption experiments show that the adsorption process is more consistent with the Langmuir equation (R^2 = 0.919, 0.916), indicating that the adsorption of rhodamine B and methylene blue by NABc1% is dominated by a monolayer adsorption process. In addition, the fitting of the intraparticle diffusion model shows that internal diffusion is not the only rate-limiting step. Hence, NABc1% has great potential for practical application as an efficient adsorbent in the field of cationic dye wastewater treatment.

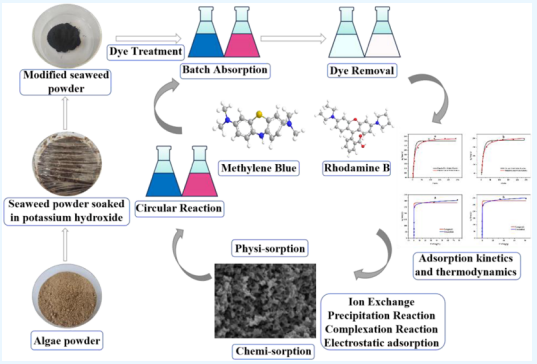

INTRODUCTION

In the past few decades, as a consequence of the swift expansion of the global population and the vigorous development of industry and agriculture, a substantial amount of waste and refuse has been discharged into water bodies. The discharge of these pollutants significantly exceeds the self-purification capacity of water bodies, thereby giving rise to serious environmental issues in the water environment.[1] Specifically, the emission of dye industry wastewater has increased dramatically. Currently, 160 million cubic meters of dye wastewater is discharged into the water environment every year in China. Most dye wastewater is well-known for its great chromaticity, high content of organic pollutants, complexity of components, and biological toxicity, as well as difficult biochemical degradation.[2] Particularly, the development of dyes with resistance to both photolysis and oxidation makes the treatment of dye wastewater even more difficult.[3] Due to a large number of organic pollutants present in printing and dyeing wastewater, they will consume dissolved oxygen, disrupting the ecological balance and endangering the survival of fish and other aquatic organisms. In addition, the further anaerobic decomposition of organic pollutants will also generate innumerable toxic species, seriously threatening the biological chain and human health.[4] Therefore, it is crucial to provide effective wastewater treatment for dye wastewater before it is discharged into the waters.

To date, various methods of dye removal have been studied and developed, including physical, chemical, and biological methods. Compared with advanced technologies such as oxidation, the Fenton process, and photocatalysis, adsorption is still a feasible method. The adsorbent has the advantages of being fast and efficient, simple preparation process, low production cost, and wide practicability. It is an effective and practical method for treating dye-contaminated water, and environmentally friendly modification methods can be selected to reduce the risk of secondary pollution of the adsorbent to the environment. In fact, the development and selection of adsorbent is greatly influenced by the nature of the dye compound (e.g., polar versus nonpolar molecules, neutral molecules versus dissociated ions) and the nature of the adsorbent surface. Currently, biochar is emerging as a novel

Received: January 11, 2025
Revised: April 20, 2025
Accepted: April 23, 2025
Published: May 1, 2025

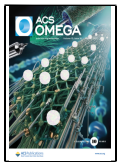

type of activated carbon, which has various advantages including rich surface functional groups, high porosity, and a large specific surface area.[5] However, compared to activated carbon, biochar as an adsorbent for the removal of dye wastewater remains at an early stage. The corresponding adsorption performance of biochar is influenced by varied factors, mainly depending on its pore structure and chemical properties. Therefore, it would be of great interest to fabricate novel functional biochar as an environmentally friendly adsorbent material, which can not only be applied for the removal of pollutants from water and atmospheric environments but also be employed in soil remediation, synthetic chemistry, and electrochemistry.[6−9]

To the best of our knowledge, the adsorption capacity of pristine unmodified biochar for dye wastewater is very poor. The adsorption capacity, selectivity, and regeneration performance of biochar can be significantly improved through modifications. The corresponding modification methods of biochar mainly include physical and chemical approaches.[10,11] Particularly, the specific surface area and the adsorption performance can be greatly enhanced through the doping of nitrogen elements.[12,13] For example, Mao et al. produced nitrogen-doped graded biochar by a combination of an ammonia roasting pretreatment and alkali activation. The results showed that the specific surface area of nitrogen-doped biochar was higher than that of nonbaking pretreatment, and the adsorption capacity of N-doped hierarchical biochar to methyl orange (MO) was the highest.[14] Zhang et al. used $K_3[Fe(C_2O_4)_3]$ as an activator to prepare magnetic self-nitrogen-doped biochar. The results showed that magnetic self-nitrogen-doped biochar has a large specific surface area and excellent adsorption capacity for Congo red and rhodamine.[15] With doping of 10% nitrogen in biochar (NBC-350-0.1), the specific surface area increased to 3.9 times that of the original biochar, and the oxygen-containing functional groups also increased significantly.[16] Accordingly, doping with varied elements is considered as an efficient approach in the fabrication of desired biochar with great adsorption properties.

Regarding this, we successfully synthesized N-doped algae biochar materials (NABc) from seaweed biomass in this work, with Dicyandiamide serving as the modifier and hydroxide acting as the activator. The structural properties of synthetic N-doped biochar were fully characterized, including the crystal structure, surface morphology, specific surface area, pore size distribution, and surface functional groups. Furthermore, the adsorption ability was also evaluated by two cationic RhB and MeB dyes. Specifically, the adsorption amounts and kinetic data were obtained. NABc1% was demonstrated to have excellent adsorption properties for the cationic dyes rhodamine B (RhB) and methylene blue (MeB). Finally, we anticipated that NABc would have great potential applications in both water treatment and environmental remediation related fields.

RESULTS AND DISCUSSION

Material Characterization. The functional groups of ABc and NABc were investigated using Fourier transform infrared (FT-IR) spectroscopy, and the results are shown in Figure 1. From the FT-IR spectra of ABc, it can be seen that the peak at 3431 cm^{-1} corresponds to the phenolic group induced −OH group stretching, while the peak at 2922 cm^{-1} corresponds to C−H stretching. The peaks at 1634 cm^{-1} correspond to C═O/C═C.[17,18] The vibrational peaks of the C−O−C are observed at 1518 cm^{-1}, while the vibration at 1033 cm^{-1} is

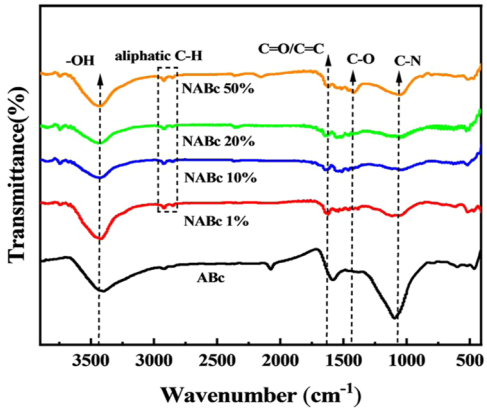

Figure 1. FT-IR spectra of ABc, NABc1, NABc10, NABc20, and NABc50%.

attributed to the C−N stretching vibrational peaks.[19,20] Compared to ABc, a slight offset value at 1634 cm^{-1} was also observed, which was attributed to the modification by Dicyandiamide and sodium hydroxide. The multiple new functional group peaks at 1300−1500 cm^{-1} also indicate that nitrogen- and oxygen-containing functional groups were introduced into the composite, thus providing more active adsorption sites. The presence of the above functional groups demonstrates the successful fabrication of NABc biochar through N doping.

The prepared samples were analyzed by an X-ray diffractometer for chemical composition and physical phase. As shown in Figure 2, ABc exhibits intense and well-defined

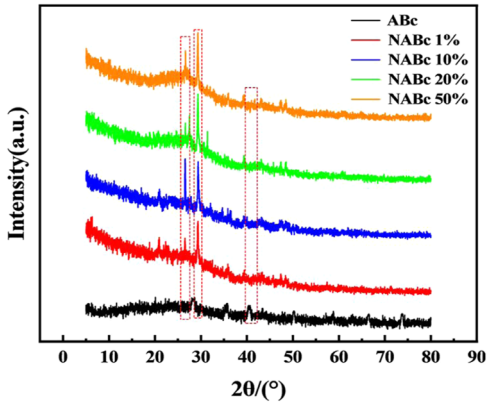

Figure 2. XRD patterns of ABc, NABc1, NABc10, NABc20, and NABc50%.

peaks corresponding to its crystal structure. Among them, the peak of 29.4 is for silicon-containing compounds. It is possible that the experimental equipment or container contains silicon (using a glass or silicon substrate) and introduces impurities into the preparation, causing silicon-containing peaks in the XRD. The sharp peak of 26.9 is the peak of graphitization, corresponding to the (002) crystal surface of graphite. Amorphous carbon may form a crystalline structure during high-temperature firing, with corresponding spikes in the XRD map.[21] The characteristic peak of C_3N_4 at 43.2° corresponds to the 102 crystal plane (PDF card number 26-1076), indicating that the graphitized crystal structure is produced after high-temperature pyrolysis. More peaks were observed for adsorbent materials treated with Dicyandiamide and NaOH.

https://doi.org/10.1021/acsomega.5c00307
ACS Omega 2025, 10, 18753−18763

This can be attributed to the fact that alkali treatment can potentially improve the resolution and intensity of the peaks in the obtained spectra.

Additionally, the specific surface area and pore structure parameters of the adsorbent were calculated by the BET method based on the N_2 adsorption/desorption isotherm.[22] The specific surface area, average hole volume, and average pore size of the prepared adsorbents are shown in Table 1. The specific surface area of ABc was 340.12 $m^2 \cdot g^{-1}$ with an average pore volume of 0.296 $cm^3 \cdot g^{-1}$ and an average pore size of 1.50 nm. After modification by Dicyandiamide, the specific surface areas of NABc all increased to different degrees. Specifically, the specific surface areas of NABc1, NABc10, NABc20, and NABc50% were 2.04, 1.55, 1.32, and 1.18 times higher than those of ABc after N doping, respectively. The mean pore sizes of NABc1, NABc10, NABc20, and NABc50% were 4.5, 4.0, 3.6, and 6.3 times larger than those of ABc, respectively. For N-modified biochar, the specific surface area decreased and the average pore volume and average pore diameter decreased and then increased with increasing amounts of modification (1−50%). The NABc1% had the largest specific surface area of 693.92 $m^2 \cdot g^{-1}$. The above BET analysis combined with the scanning electron microscopy results suggests that a well-developed carbon skeleton structure was sufficiently constructed in NABc1%, which may facilitate the excellent removal and attachment of dye molecules to the synthesized samples.

Table 1. BET Data for ABc, NABc1, NABc10, NABc20, and NABc50%.

samples	S_{BET} $(m^2 \cdot g^{-1})^a$	$V_{Average}$ $(cm^3 \cdot g^{-1})^b$	$S_{average}$ $(nm)^c$
ABc	340.12	0.296	1.50
NABc1%	693.92	0.162	6.76
NABc10%	527.15	0.143	6.02
NABc20%	451.16	0.131	5.38
NABc50%	403.12	0.139	9.51

[a]Specific surface area. [b]Average hole volume. [c]Average pore size.

The structure and morphology of biochar mainly depend on the feedstock and carbonization conditions, which affect its

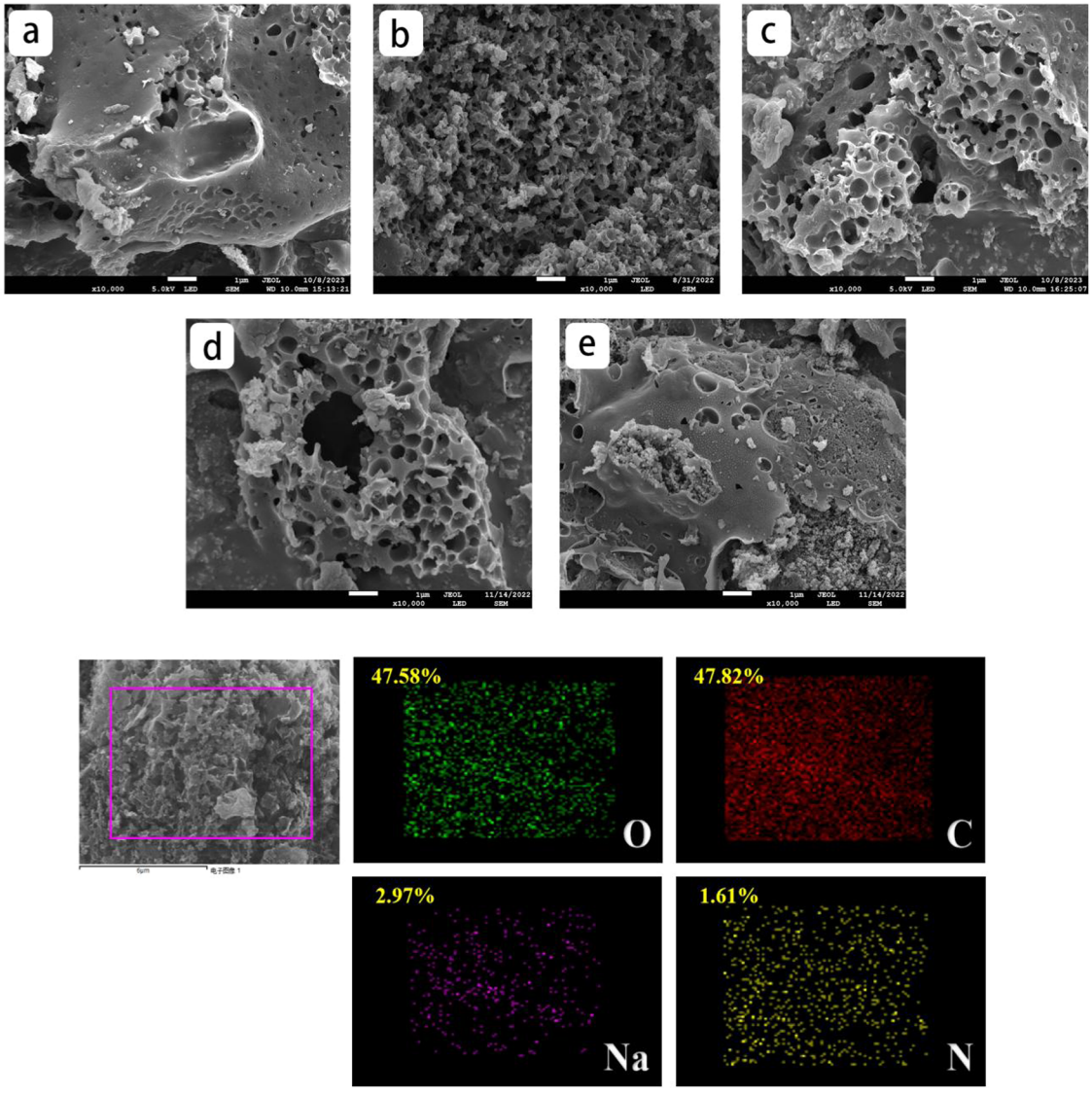

Figure 3. SEM images of ABc (a), NABc1% (b), NABc10% (c), NABc20% (d), and NABc50% (e), and EDS spectrum patterns of NABc1%.

https://doi.org/10.1021/acsomega.5c00307
ACS Omega 2025, 10, 18753−18763

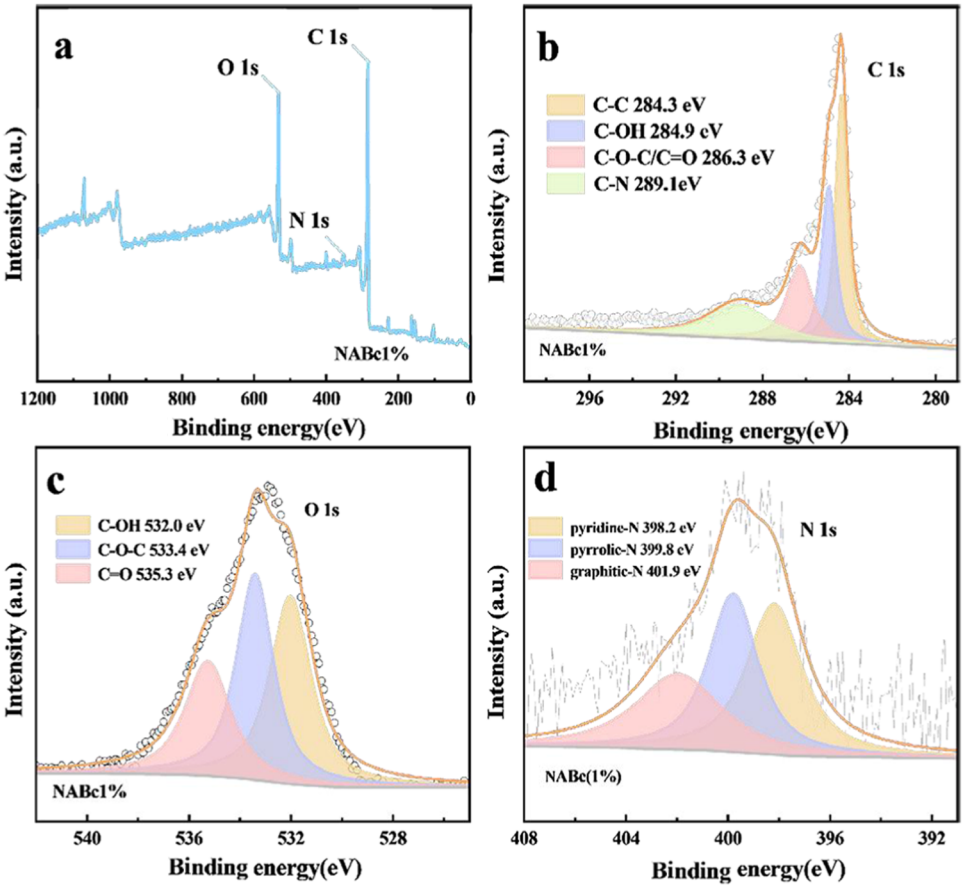

Figure 4. Full spectrum of C (a); C 1s XPS analysis of NABc1% (b); O 1s XPS analysis of NABc1% (c); and N 1s XPS analysis of NABc1% (d).

adsorption properties for dyes. Figure 3 shows the scanning electron microscopy images of ABc (Figure 3(a)) and N-doped modified ABc (Figure 3(b−e)). The surface of ABc was smooth with no obvious pore structure, and a small number of tiny irregular particles were dispersed on its surface (Figure 3(a)). The surface of N-modified ABc composites (Figure 3(b−e)) showed obvious pore, interstitial, and pore honeycomb microcavity-like structures with abundant stomata. This may be related to the etching effect of sodium hydroxide and gas generation from the decomposition of Dicyandiamide during pyrolysis.[23,24] Pores are desirable because they increase the adsorption of cationic dyes by providing more adsorption active centers. The surface pore structure of NABc1% was the most developed (Figure 3(b)), which is in agreement with the results of the BET tests. According to the BET data, compared with NABc1%, the surface area of NABc10, NABc20, and NABc50% decreased significantly, and the pore volume also decreased significantly. This may be due to the increase of the doping amount of Dicyandiamide, which caused pore blockage during pyrolysis. The rich pore structure can effectively increase the adsorption capacity of the adsorbent for pollutants. Therefore, the prepared samples had an ordered, uniform, and developed honeycomb structure, which is favorable for the high physical adsorption performance of cationic dyes and can be considered a low-cost and easily accessible biosorbent for wastewater treatment. From the energy dispersive X-ray spectroscopy (EDS) spectra, it can be seen that the oxygen element content on the surface of NABC is 47.58%, indicating that the modified biochar surface has abundant oxygen-containing functional groups. The Na element content is 2.97%, and the N element content is 1.61%, which fully demonstrates the successful doping of N elements into the structure of seaweed biochar during the modification process.

In order to further analyze the elemental composition of the prepared adsorbent, NABc1% was characterized by X-ray photoelectron spectroscopy (XPS). As shown in Figure 4(a), the XPS spectrum of NABc1% shows three characteristic peaks at 283.7, 398.4, and 531.6, corresponding to C 1s, O 1s, and N 1s, respectively. These results prove that there are C, O, and N elements in NABc1%. By fitting the corresponding XPS high-resolution spectra, the chemical composition and chemical oxidation states of C, O, and N elements in NABc1% adsorbent can be revealed. The XPS spectra of C 1s can be decomposed into four types of peaks (Figure 4(b)): non-oxidized carbon atom C−C (284.3 eV), carbon atom of C−OH bond (284.9 eV), carbon atom of C−O−C/C═O bond (286.3 eV) and carbon atom of C−N bond (289.1 eV). In the C 1s spectrum, the peak proportions of the areas of C−O, C−O, O═C−O, and C−N were 32.7, 24.1, 21.1, and 22.1%, respectively. The O 1s peak fitting results of NABc1% have three main peaks at 532.0, 533.4, and 535.3 eV (Figure 4(c)), which are attributed to C−OH, C−O−C, and C═O, respectively. In the O 1s spectrum, the peak proportions of the areas of C−OH, O−C−O, and C═O were 37.5, 37.3, and 25.4%, respectively. The N 1s peak fitting results of NABc1% have three main peaks at 401.9, 399.8, and 398.2 eV (Figure 4(d)), which are attributed to graphite nitrogen, pyrrole nitrogen, and pyridine nitrogen, respectively. In the highly resolved N 1s spectrum, the peak proportions of the areas of

https://doi.org/10.1021/acsomega.5c00307
ACS Omega 2025, 10, 18753−18763

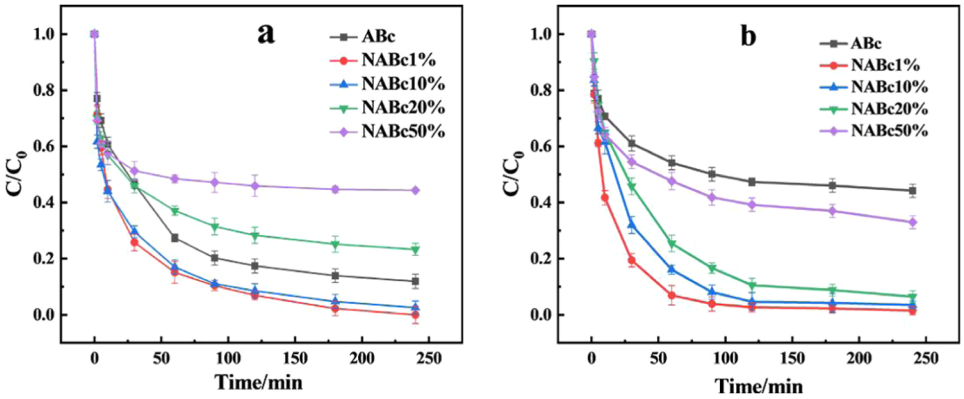

Figure 5. Removal effect of RhB (a) and MeB (b) by different doping ratios.

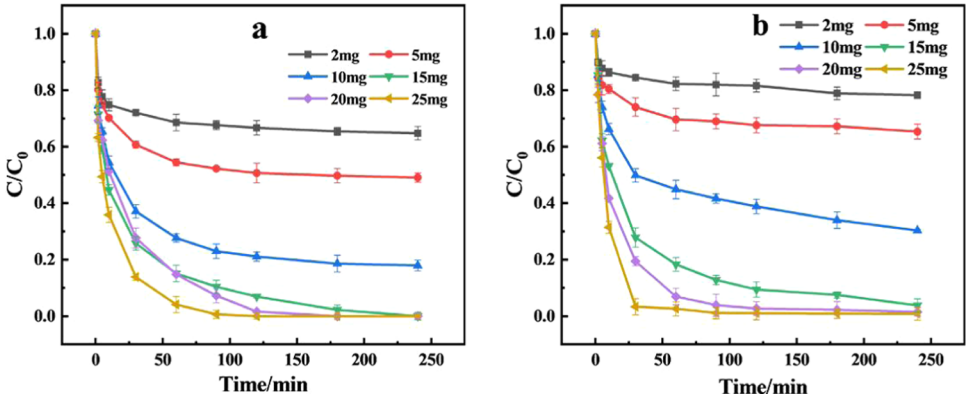

Figure 6. Removal effects of RhB (a) and MeB (b) with different addition amounts.

graphite nitrogen, pyrrole nitrogen, and pyridine nitrogen were 28.3, 34.8, and 36.9%, respectively. XPS results further confirmed the successful synthesis of NABc1%.

Adsorption Experiment. To compare the effect of Dicyandiamide addition on the adsorption of cationic dyes and to find the most suitable loading, the removal efficiencies of algal biochar impregnated with different Dicyandiamide additions for RhB and MeB are shown in Figure 5. The removal effect of the amount of Dicyandiamide added to the adsorbent on RhB is shown in Figure 5a. Biochar without added Dicyandiamide (ABc) showed a long adsorption time (240 min) for complete adsorption of RhB. Compared with ABc, NABc1% showed the shortest time of 120 min for complete adsorption of RhB. However, the adsorption efficiency and removal rate of RhB by NABc10 and NABc50% materials were significantly lower than that of ABc, which indicated that the removal rate of RhB by the modified materials was affected by the addition of Dicyandiamide. NABc1% had the best adsorption effect on RhB, but the adsorption effect became worse with an increase in the additional amount. The adsorption of MeB by Dicyandiamide addition in the adsorbent showed the same pattern (see Figure 5b). NABc1% had the best removal efficiency on MeB with 96.2%, which was significantly stronger than that of unmodified ABc. With the increase of Dicyandiamide doping, the adsorption and removal effects became worse and lower than those of ABc. The removal efficiency of NABc50% for MeB was only 61.8%. Therefore, the loading value of NABc was set at 1% in the following experiments because NABc1% had the highest adsorption and removal efficiency for RhB and MeB. Therefore, an appropriate amount of Dicyandiamide doping can introduce more chemisorption sites on the surface of NABc biochar, and these introduced chemisorption sites will be favorable for the adsorption of cationic dyes. In summary, with the increase in doping amount, the removal efficiency decreases. It may be because the excessive doping of Dicyandiamide leads to blockage of the pore structure, resulting in a decrease in the surface area and a large number of reactive sites. This is consistent with the results of BET. The removal effects of RhB and MeB with different addition amounts are shown in Figure 6. From Figure 6(a), it can be seen that the removal of RhB increased with the increase of NABc1% addition. When the addition amount is 15 mg, the removal rate of RhB for 90 min is 99.4%; when the addition amount exceeds 15 mg, the removal rate does not change. Figure 6(b) shows that the removal of methyl bromide increased with the addition of NABc1%. When the addition amount is 15 mg, the removal rate of MeB is 96.2% after 90 min of reaction. When the addition amount exceeded 20 mg, the removal rate did not change significantly. The removal rate increased with the increase in adsorbent dose. This is mainly due to the increase of effective adsorption sites with the increase of dose under the condition of a constant dye concentration. The adsorption effect of NABc1% on RhB and MeB is much higher than that of ABc, which may be due to the large number of functional groups on the surface of modified NABc1%, which will greatly promote the adsorption of cationic dyes through complexation. In order to compare the experiment better, an additional

https://doi.org/10.1021/acsomega.5c00307
ACS Omega 2025, 10, 18753−18763

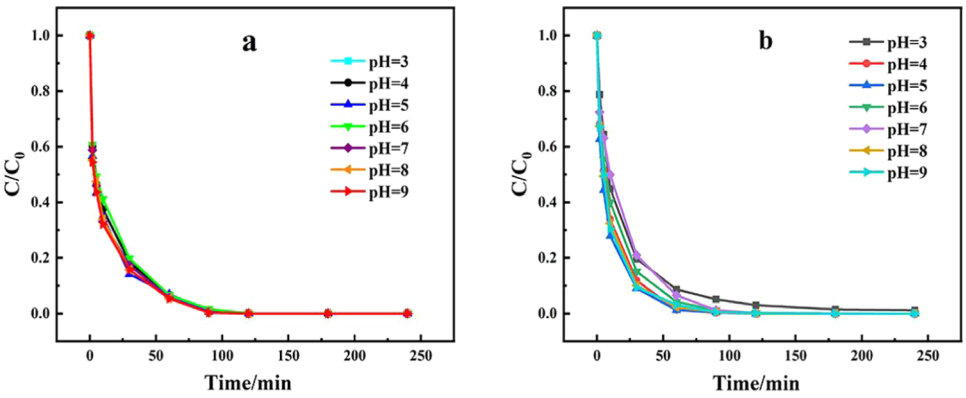

Figure 7. Removal effect of RhB (a)and MeB (b) at different pH values.

amount of 15 mg is selected as the best experimental condition.

The removal effects of RhB and MeB at different pH values are shown in Figure 7. With the change in pH value, the removal rate of RhB basically remained unchanged, and after 90 min of reaction, the removal rate of RhB reached the highest. The removal of MeB varied negligibly with pH, reaching a maximum after 180 min of reaction. The experimental results showed that the pH values of RhB and MeB solutions had no significant effect on the adsorption of the NABc1% composites. The results of pH showed that the effect of pH on the adsorption of RhB by NABc1% was not significant, indicating that NABc1% had a wide application range for the system. When pH = 3−9, it has little effect on the adsorption of MeB by NABc1%. When pH = 3, the removal efficiency of MeB by NABc1% was slightly lower in the first 100 min. It may be because when pH = 3, there is a large amount of H^+ in the system, which forms competitive adsorption with cationic dyes. When pH = 9, the removal efficiency of MeB by NABc1% was the highest. It may be because, as the pH value of the system increases, the electronegativity of the NABc1% surface gradually increases, with a large amount of negative charge, forming electrostatic attraction with the cationic dye, increasing the removal efficiency. The pHpzc of the composite was estimated to be 3.8 by the relationship between ζ-potential and pH (Figure 8). At pH < 3.8, the surface of NABc1% is positively charged. At pH > 3.8, the surface of NABc1% is negatively charged. This behavior is related to protonation and deprotonation, respectively.

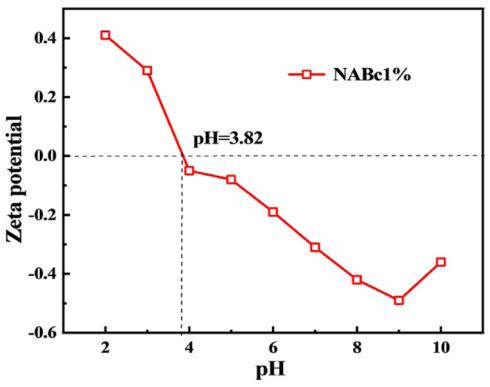

Figure 8. ζ-Potential of NABc1%.

The removal effects of RhB and MeB at different temperatures are shown in Figure 9. It can be seen from Figure 9(a) that with the increase in temperature, the adsorption effect of NABc1% composites on RhB improves, but the effect of the temperature on adsorption and removal efficiency is not significant. The adsorption effect of NABc1% composites on RhB and MeB is improved by increasing the temperature. The reason may be that under high temperature conditions, the surface active sites of biochar are more active, making it easier to interact with dye molecules, which is conducive to the adsorption process, and high temperature will promote the diffusion rate of adsorbate in solution and improve the adsorption efficiency. The influence of the temperature on the adsorption of MeB by adsorbents follows the same pattern in the environment (Figure 9(b)). The pH and temperature had little effect on the system, and the effect of pH and temperature changes on the adsorption of NABc1% was not considered in subsequent experiments. Table 2 shows the comparison of different parameters such as the dosage of adsorbent in different literature studies.

Adsorption Kinetics. The adsorption kinetic model of NABc1% composites for RhB adsorption is shown in Figure 10(a), and the fitting parameters are shown in Table 3. The fitting parameter R^2 of the quasi-second-order kinetic model is 0.961, which is higher than that of the quasi-first-order kinetic model (R^2 = 0.876). The adsorption kinetic model fitting of MeB adsorbed on NABc1% composites is shown in Figure 10(b), and the fitting parameters are shown in Table 3. The fitting parameter R^2 of the quasi-second-order kinetic model is 0.998, which is higher than that of the quasi-first-order kinetic model (R^2 = 0.979). It is concluded that the quasi-second-order kinetic equation can better describe the whole process of adsorption of RhB and MeB solution by NABc1% composites.[30,31]

Adsorption isotherms can describe the relationship between the equilibrium mass concentration of RhB and MeB solutions and the adsorption capacity of NABc1% composites and reveal the interaction between NABc1% composites and RhB and MeB solution. Figure 11 shows the adsorption isotherm fitting of NABc1% composites to RhB and MeB solutions, and Table 4 shows the isotherm fitting data of NABc1% composites. It can be seen from Figure 11 that the adsorption of RhB and MeB solution by NABc1% composites is in good agreement with the Langmuir model equation. It shows that the adsorption of RhB and MeB solution by NABc1% composites tends to be monolayer adsorption.[32,33] The Gibbs free energies of the RhB and MeB adsorption reactions were calculated at

https://doi.org/10.1021/acsomega.5c00307
ACS Omega 2025, 10, 18753−18763

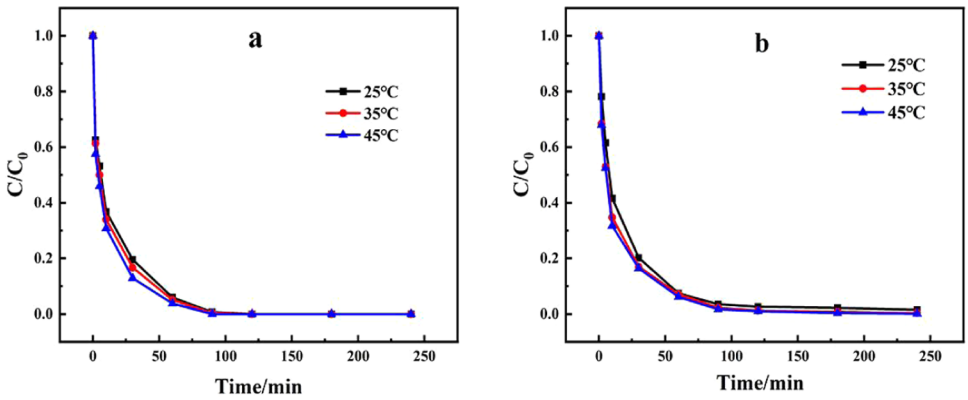

Figure 9. Removal effects of RhB (a) and MeB (b) at different temperatures.

Table 2. Comparison of Adsorbent Dosage and Other Conditions in Different Literatures

biomass	doped materials/method	adsorbent dosage	concentration (pollutant)	pH	reaction time and efficiency
straw[25]	TiO_2	0.025 g	20 mg/L RB (100 mL)	7	200 min 100%
rice-bran[26]	ball-milling	0.050 g	10 μM RB (50 mL)		12 min 82%
oil palm empty fruit bunches[27]	KOH	0.010 g	50 mg/L (50 mL)	6	180 min 93.66%(MeB) 94.68%(RB)
eggshell membrane[28]	KOH/HNO_3	0.025 g	100 mg/L (20 mL)	9	240 min 96%
fennel seeds[29]		0.025 g	20 mg/L (50 mL)	7	24 h ≈97%
seaweed (this work)	dicyandiamide	0.015 g	100 mg/L RB/MeB (50 mL)	7	90 min 99.4%(RB) 96.2%(MeB)

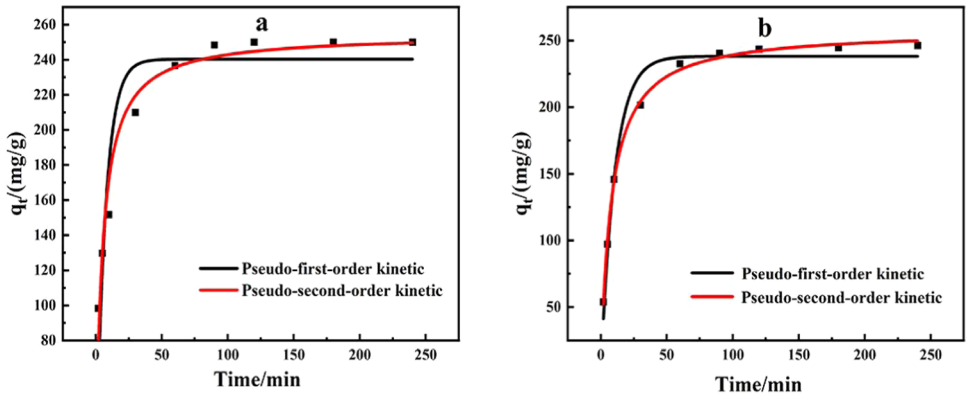

Figure 10. Kinetic fitted curves of the adsorption kinetics of NABc1% on RhB (a) and MeB (b).

Table 3. Fitting Parameters of the Adsorption Kinetic Models of NABc1% in RhB and MeB

	quasi-first-order kinetic			quasi-second-order kinetic model		
samples	Q_E (mg·g^{-1})	k_1 (min^{-1})	R^2	Q_E (mg·g^{-1})	K_2 [g/(mg·min^{-1})]	R^2
RhB	240.3	0.139	0.876	254.6	8.16×10^{-4}	0.961
MeB	238.2	0.095	0.979	257.9	4.93×10^{-4}	0.998

various temperatures. As can be seen from Table 5, the Gibbs free energy is less than 0, and the Gibbs free energy corresponding to both dyes shows a trend of becoming smaller, indicating that the adsorption of this biochar surface is spontaneous. The higher the temperature, the smaller the value of ΔG^0, the higher the degree of spontaneous reaction, and the warming facilitates the progress of the reaction. Removal of both RhB and MeB may be a thermodynamically favorable process.

The intraparticle diffusion model can also be used to explain the diffusion mechanism in the adsorption process. Table 6 shows the fitting data of intraparticle diffusion. The adsorption

https://doi.org/10.1021/acsomega.5c00307
ACS Omega 2025, 10, 18753−18763

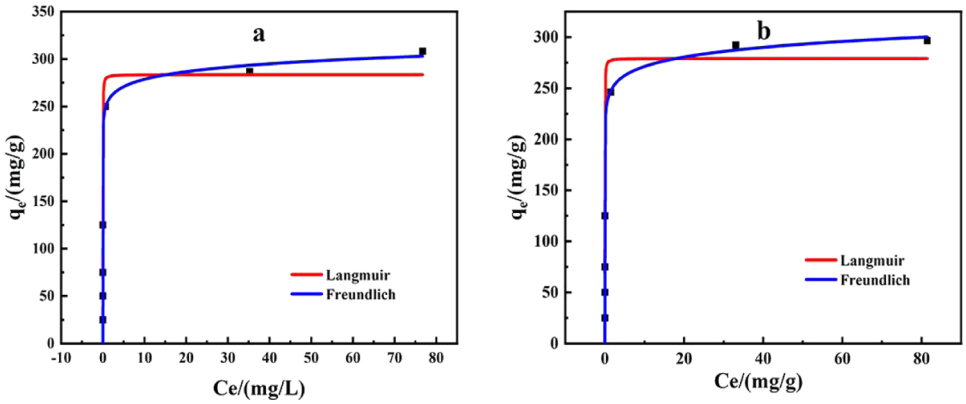

Figure 11. Adsorption isotherm fitting of RhB (a) and MeB (b) adsorbed by NABc1%.

Table 4. Adsorption Isotherm Fitting Data of NABc1%

	Langmuir model			Freundlich model		
samples	q_m (mg/g)	k_L (L/mg)	R^2	k_F (mg/g)	n_F	R^2
RhB	19,311	68.09	0.919	253.54	0.041	0.712
MeB	19,111	68.46	0.916	242.82	0.048	0.703

Table 5. Gibbs Free Energy at Different Temperatures

	ΔG^0 (KJ mol^{-1})		
samples	25° (298 K)	35° (308 K)	45° (318 K)
RhB	−26.77	−30.10	−33.05
MeB	−11.61	−15.91	−19.34

process is divided into three stages. It can be seen from Figure 12 that C ≠ 0, the fitting curve does not pass through the zero point, indicating that the internal diffusion is not its only rate-limiting step. $k_1 > k_2 > k_3$, indicating that the adsorption sites on the adsorbent are occupied by the adsorbed substances. So the adsorption rate will slow down and eventually reach equilibrium. In the rapid adsorption stage, the k_1 value is the highest, indicating that the dye has the strongest adsorption capacity when it is quickly adsorbed to the outer surface of the biochar. In the internal diffusion stage, intraparticle diffusion becomes the main reason for limiting the adsorption rate, and the dye molecules adsorbed on the outer surface of the biochar slowly enter the pores. In the adsorption equilibrium stage, the k_3 value is the smallest. At this time point, the adsorption sites on the biochar are completely occupied, and the adsorption stops. This shows that the adsorption process is accompanied by other adsorption mechanisms.

Recyclability Experiment. Reusability is an important index to evaluate whether the adsorbent has a practical application value. As shown in Figure 13, the adsorption efficiency of NABc1% decreased to varying degrees after 5 cycles, which may be due to the fact that some adsorption sites of NABc1% were not completely desorbed. Overall, after 5 cycles, the adsorption efficiency of NABc1% for RhB and MeB remained at about 80%, indicating that the adsorbent has good stability and reusability.

FUTURE PROSPECTS

As an economical and friendly adsorbent, biochar can remove dyes from industrial wastewater and can be used as an alternative to other expensive adsorbents. However, the composition of the actual dye wastewater is more complex than that of the simulated dye wastewater in this experiment. In the practical application process, it is necessary to consider the control of realistic factors, such as reaction conditions and operating costs. These factors may have a certain limiting effect on dye removal, which requires further discussion and research. In this study, although NABc1% has good material stability and can still achieve a good removal effect after repeated use, it has encountered problems such as difficult material collection and large loss in the recovery process in the actual process. Therefore, the development of a more effective material collection method is an important research direction for the future.

CONCLUSIONS

In summary, NABc biochar composites were successfully prepared by adding N to the surface of algal biochar by impregnation and calcination methods. Particularly, the rich pore structure of NABc1% effectively improved the adsorption capacity of the adsorbent for cationic dyes. The adsorption of cationic dyes in NABc1% is minimally affected by the pH and temperature. When the addition amount is 15 mg, the temperature is 25 °C, and the pH is 7, the removal rate of RhB by NABc1% is 99.4% and the removal rate of MeB is 96.2%. The adsorption of cationic dyes accords with the pseudo-second-order adsorption kinetic model, which shows that chemisorption is dominant in the adsorption process. These results provide new ideas for the preparation of low-cost, effective, and promising biosorbents for the adsorption of cationic dyes. Finally, we expect a potential application of NABc1% in the treatment of cationic dye wastewater.

Table 6. Adsorption Isotherm Fitting Data of NABc1%[a]

	K_1	C	R^2	K_2	C	R^2	K_3	C	R^2
RhB	30.438	57.451	0.963	9.715	158.115	0.959	0.109	248.281	0.947
MeB	52.521	20.309	0.999	9.892	149.951	0.866	0.634	236.274	0.932

[a] K_1: Mg/g min$^{0.5}$, C: Mg/g.

https://doi.org/10.1021/acsomega.5c00307
ACS Omega 2025, 10, 18753−18763

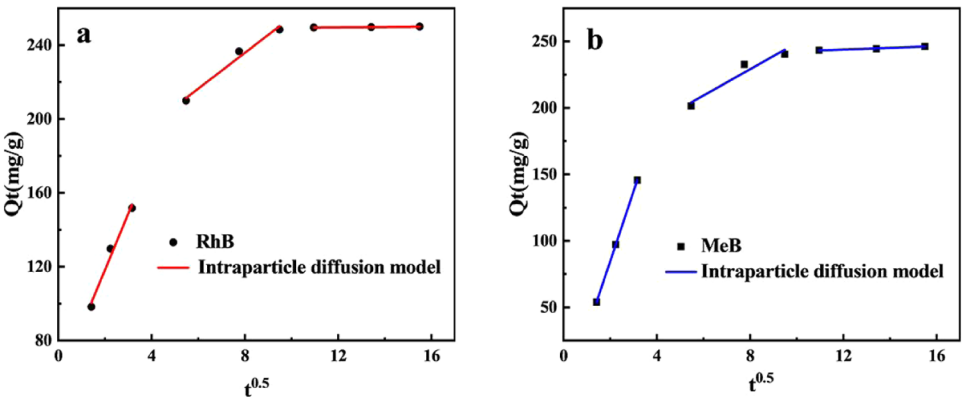

Figure 12. Adsorption isotherm fitting of RhB (a) and MeB (b) adsorbed by NABc1%.

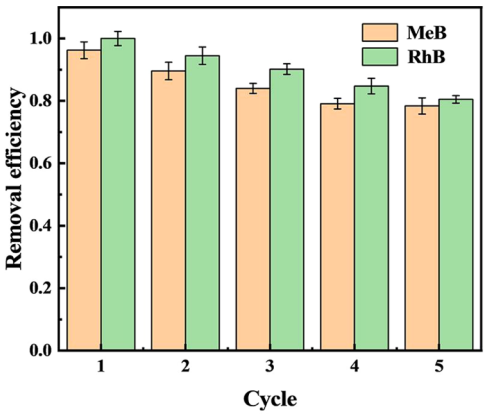

Figure 13. RhB and MeB adsorption recycles on NABc1%.

MATERIALS AND METHODS

Dicyandiamide (AR) and rhodamine B (RhB) were obtained from Shanghai McLean Biochemical Technology Co., Ltd.. Methylene blue (MeB) was ordered from Tianjin Guangfu Fine Chemical Plant. Sodium hydroxide (AR, ≥96%) was shipped from the Guangzhou Chemical Reagent Factory. Potassium hydroxide (AR, ≥85%) was shipped from Guangzhou Chemical Reagent Factory. Hydrochloric acid (HCl, 36−38%) was purchased from Xilong Science Co., Ltd.. Simulated samples of cationic dye wastewater with different concentrations were prepared by using various dyes in the lab. Brown algae was collected from Guilin Ocean Beach, Haikou City.

Synthesis of the ABc/NABc Materials. Seaweed powder (5.0 g), KOH (15.0 g), and deionized water (50 mL) were placed in a 100 mL glass beaker. The mixture was stirred for 2 h under magnetic conditions at the room temperature. The mixed material was dried in an oven at 80 °C. After being calcined at 700 °C for 270 min under nitrogen conditions, the sample was washed alternately by deionized water and ethanol to neutral pH (pH = 7) and then placed in a vacuum oven at 70 °C for drying. The product seaweed biochar (ABc) was obtained.

N-doped algal biochar was synthesized by an impregnation method. NaOH (0.20 g) and Dicyandiamide (0, 0.02, 0.20, 0.40, 1.00 g) were added into 30 mL of distilled water, respectively, which were shaken at 50 °C for over 1 h. Then 2.00 g of brown algae was added, and the mixture was dispersed by ultrasonic waves. After being dried at 70 °C in a vacuum oven, the sample was heated up to 550 °C (10 °C·min^{-1}) under nitrogen protection over 2 h. Typically, the N-doped seaweed biochars (ABc, NABc1, NABc10, NABc20, and NABc50%) were prepared after washing with distilled water, which was ground and passed through 200 mesh sieves.

Characterization of the ABc/NABc Materials. Field emission scanning electron microscopy (SEM, JSM-7401F, Jeol Company, Japan) was used to characterize the surface morphologies of the materials. The functional groups on the surface of the material were characterized by Fourier transform infrared spectroscopy (FT-IR6700, American Thermo Company). Raman spectroscopy was used to detect the number of functional groups and the degree of graphitization of the adsorbent, with a range of 500−2000 cm^{-1}. The specific surface area and pore size of the material were evaluated by adsorption and desorption specific surface area pore size distribution instruments (ASAP2460, American Micromeritics Company). The concentration of cationic dyes was determined by a UV−vis spectrophotometer (752N, Shanghai Youke Instrument Co., Ltd.).

Adsorption Experiments. Adsorption kinetics of RhB and MeB were carried out with batch experiments, separately. The stock solutions of RhB and MeB (100 mg·L^{-1}) were prepared initially. Specifically, the pH was adjusted to 7.0 ± 0.1 with NaOH (0.01 mol·L^{-1}) or HCl (0.01 mol·L^{-1}). The solution samples were taken in a timely manner and filtered with 0.45 μm membranes. The residual RhB and MeB were detected with a UV−vis spectrophotometer at 554 and 610 nm, respectively, and the corresponding concentrations were calculated according to the standard curves established. Additionally, the adsorbents were collected by centrifugation at the end of the tests and washed twice with 40 mL of deionized water. The collected adsorbents were dried at 75 °C for FT-IR detection. The quasi-first-order (1) and quasi-second-order adsorption kinetics (2) models were used to simulate the adsorption process, respectively.[34,35]

$$q_t = q_e(1 - e^{-k_1 t}) \quad (1)$$

$$q_t = k_e q_e^{\,2} t/(1 + k_2 q_e t) \quad (2)$$

where q_e is the equilibrium adsorption capacity, mg·g^{-1}; q_t is the amount of adsorption at t, mg·g$^{-1;}$ k_1 and k_2 are quasi-first-order and quasi-second-order adsorption rate constants, min^{-1} and g·(mg·min)$^{-1}$, respectively.

Following the same procedure above, a series of initial concentrations of rhodamine B and methylene blue were settled from 0 to 200 mg·L^{-1}, respectively. According to the

https://doi.org/10.1021/acsomega.5c00307
ACS Omega 2025, 10, 18753−18763

detected residual concentration at adsorption equilibriums, the adsorption isotherms were established.[36,37] Freundlich and Langmuir isothermal adsorption models are shown in formulas (3) and (4)

$$q_e = K_F C_e^{1/n} \quad (3)$$

$$q_e = (q_{max} K_L C_e)/(1 + K_L C_e) \quad (4)$$

where C_e is the mass concentration of the solution at the adsorption equilibrium of the composite material, mg·L^{-1}; q_e is the equilibrium adsorption capacity of a composite solution, mg·g^{-1}; q_{max} is the theoretical maximum adsorption capacity of the solution adsorbed by the composite material, mg·g^{-1}; K_f and K_L are Freundlich and Langmuir adsorption constants, respectively.

The intraparticle model assumes that the adsorption rate depends on the solid adsorbent properties. The expression of the linearized model is as follow

$$Q_t = K_p t^{1/2} + C \quad (5)$$

where Q_t is the adsorption amount at time t and k_p is the intraparticle diffusion rate constant.

Additionally, one-factor experiments were carried out to evaluate the effects of sorbents, adsorbent dosage, and pH on the removal of RhB and MeB (100 mg·L^{-1}). As for the sorbent effect evaluation, 20 mg of ABc, NABc1, NABc10, NABc20, and NABc50% were added into 50 mL of RhB and MeB (100 mg·L^{-1}) aqueous solution and shaken at room temperature for 240 min, respectively. Similarly, the adsorbent amount ranged from 2 mg to 25 mg, and a series of pH levels were adjusted with NaOH (0.01 M) and HCl (0.01%). Samples were taken after the adsorption equilibrium concentrations of the residual dyes were detected, and removal efficiency was calculated.

Recyclability Experiment. A 15 mg portion of NABc1% was added to 100 mg/L MeB and RhB solutions, respectively. After adsorption, the sample was desorbed in a 0.003 mmol/L H_2O_2 solution for 1 h. The samples were washed with deionized water and centrifuged and then dried in a constant temperature oven at 60 °C for 6 h. These steps were repeated 4 times.

AUTHOR INFORMATION

Corresponding Author

Xianghui Wang − *Key Laboratory of Water Pollution Treatment and Resource Reuse of Hainan Province, Key Laboratory of Soil Pollution Remediation and Resource Reuse of Haikou City, College of Chemistry and Chemical Engineering, Hainan Normal University, Haikou, Hainan 571158, China*; Email: god820403@163.com

Authors

Meiyuan Fu − *Key Laboratory of Water Pollution Treatment and Resource Reuse of Hainan Province, Key Laboratory of Soil Pollution Remediation and Resource Reuse of Haikou City, College of Chemistry and Chemical Engineering, Hainan Normal University, Haikou, Hainan 571158, China*; orcid.org/0009-0003-4243-5256

Jia Xu − *Lianghu School, Daqing, Heilongjiang 163711, China*

Tiantian Lu − *Experimental School of Dezhou Ningjin County New Town, Dezhou, Shandong 253400, China*

Qianhui Ma − *Key Laboratory of Water Pollution Treatment and Resource Reuse of Hainan Province, Key Laboratory of Soil Pollution Remediation and Resource Reuse of Haikou City, College of Chemistry and Chemical Engineering, Hainan Normal University, Haikou, Hainan 571158, China*

Yun Luo − *Key Laboratory of Water Pollution Treatment and Resource Reuse of Hainan Province, Key Laboratory of Soil Pollution Remediation and Resource Reuse of Haikou City, College of Chemistry and Chemical Engineering, Hainan Normal University, Haikou, Hainan 571158, China*

Wen Feng − *Key Laboratory of Water Pollution Treatment and Resource Reuse of Hainan Province, Key Laboratory of Soil Pollution Remediation and Resource Reuse of Haikou City, College of Chemistry and Chemical Engineering, Hainan Normal University, Haikou, Hainan 571158, China*

Complete contact information is available at: https://pubs.acs.org/10.1021/acsomega.5c00307

Author Contributions

Investigation, data curation, methodology, writing—original draft, M.F.; formal analysis, software, J.X.; investigation, methodology, software, T.L.; formal analysis, supervision, validation, funding acquisition, W.F.; formal analysis, software, Y.L.; supervision, validation, Q.M.

Notes

The authors declare no competing financial interest.

ACKNOWLEDGMENTS

This work is funded by the Hainan Province Science and Technology Special Fund grant number ZDYF2022XDNY158, Hainan Provincial Natural Science Foundation of China grant number 221MS035, and College Students Innovation Project, grant number hscx2023-27 and 202311658014.

REFERENCES

(1) Praveen, S.; Jegan, J.; Pushpa, T. B.; Gokulan, R.; Bulgariu, L. Biochar for removal of dyes in contaminated water: an overview. *Biochar* **2022**, *4*, No. 10.

(2) Khan, A. A.; Gul, J.; Naqvi, S. R.; Ali, I.; Farooq, W.; Liaqat, R.; AlMohamadi, H.; Štěpanec, L.; Juchelková, D. Recent progress in microalgae-derived biochar for the treatment of textile industry wastewater. *Chemosphere* **2022**, *306*, No. 135565.

(3) Issaka, E.; Fapohunda, F. O.; Amu-Darko, J. N. O.; Yeboah, L.; Yakubu, S.; Varjani, S.; Ali, N.; Bilal, M. Biochar-based composites for remediation of polluted wastewater and soil environments: Challenges and prospects. *Chemosphere* **2022**, *297*, No. 134163.

(4) Saeed, A. A. H.; Harun, N. Y.; Sufian, S.; Siyal, A. A.; Zulfiqar, M.; Bilad, M. R.; Vaganantha, A.; Al-Fakih, A.; et al. Eucheuma cottonii Seaweed-Based Biochar for Adsorption of Methylene Blue Dye. *Sustainability* **2020**, *12* (24), No. 10318.

(5) Xiang, W.; Zhang, X. Y.; Chen, J. J.; Zou, W. X.; He, F.; Hu, X.; Tsang, D. C. W.; Ok, Y. S.; Gao, B. Biochar technology in wastewater treatment: A critical review. *Chemosphere* **2020**, *252*, No. 126539.

(6) Sutar, S.; Patil, P.; Jadhav, J. Recent advances in biochar technology for textile dyes wastewater remediation: A review. *Environ. Res.* **2020**, *209*, No. 112841.

(7) Lin, S. L.; Zhang, H. J.; Chen, W. H.; Song, M. J.; Kwon, E. E. Low-temperature biochar production from torrefaction for wastewater treatment: A review. *Bioresour. Technol.* **2023**, *387*, No. 129588.

(8) do Nascimento, Í. V.; Fregolente, L. G.; de Araújo Pereira, A. P.; do Nascimento, C. D. V.; Mota, J. C. A.; Ferreira, O. P.; de Freitas Sousa, H. H.; da Silva, D. G. G.; et al. Biochar as a carbonaceous material to enhance soil quality in drylands ecosystems: A review. *Environ. Res.* **2023**, *233*, No. 116489.

(9) Saravanan, A.; Kumar, P. S. Biochar derived carbonaceous material for various environmental applications: Systematic review. *Environ. Res.* **2022**, *214*, No. 113857.

(10) Foong, S. Y.; Chan, Y. H.; Chin, B. L. F.; Lock, S. S. M.; Yee, C. Y.; Yiin, C. L.; Peng, W. X.; Lam, S. S. Production of biochar from rice straw and its application for wastewater remediation−An overview. *Bioresour. Technol.* **2022**, *360*, No. 127588.
(11) Rawat, S.; Mishra, R. K.; Bhaska, T. Biomass derived functional carbon materials for supercapacitor applications. *Chemosphere* **2022**, *286*, No. 131961.
(12) Liu, X.-J.; Li, M.; Singh, S. Manganese-modified lignin biochar as adsorbent for removal of methylene blue. *J. Mater. Res. Technol.* **2021**, *12*, 1434−1445.
(13) Behera, A. K.; Shadangi, K.; Sarangi, P. Efficient removal of Rhodamine B dye using biochar as an adsorbent: Study the performance, kinetics, thermodynamics, adsorption isotherms and its reusability. *Chemosphere* **2024**, *354*, No. 141702.
(14) Mao, Y. T.; Cai, B.; Huang, M.; Liu, X. H.; Zhang, W. B.; Ma, Z. Q. A sustainable preparation strategy for the nitrogen-doped hierarchical biochar with high surface area for the enhanced removal of organic dye. *Biochar* **2023**, *5*, No. 70.
(15) Zhang, X. Y.; Tran, H. N.; Liu, Y. N.; et al.*et al.* Nitrogen-doped magnetic biochar made with $K_3[Fe(C_2O_4)_3]$ to adsorb dyes: Experimental approach and density functional theory modeling. *J. Cleaner Prod.* **2023**, *383*, No. 135527.
(16) Jiang, S.; Yan, L.; Wang, R.; Li, G.; Rao, P.; Ju, M.; Jian, L.; Guo, X.; Che, L. Recyclable nitrogen-doped biochar via low-temperature pyrolysis for enhanced lead(II) removal. *Chemosphere* **2022**, *286*, No. 131666.
(17) Chen, J. W.; Zanli, B. L. G. L.; Tang, W. N-doped and activated porous biochar derived from cocoa shell for removing norfloxacin from aqueous solution: Performance assessment and mechanism insight. *Environ. Res.* **2021**, *214*, No. 113951.
(18) Fan, J. P.; Li, Y.; Yu, H. Y.; Li, Y. X.; Yuan, Q. J.; Xiao, H. L.; Li, F. F.; Pan, B. U-sing sewage sludge with high ash content for biochar production and Cu(II) sorption. *Sci. Total Environ.* **2020**, *713*, No. 136663.
(19) Wu, D.; Chen, Q.; Wu, M.; Zhang, P.; He, L.; Chen, Y.; Pan, B. Heterogeneous compositions of oxygen-containing functional groups on biochars and their different roles in rhodamine B degradation. *Chemosphere* **2022**, *292*, No. 133518.
(20) Xiang, J.; Luo, B. X.; Li, J. M.; Mi, Y.; Tiam, B.; Gong, S. J.; Zhou, Y. R.; Ma, T. W. Development of KOH and H_3PO_4-modified composite biochar from corn straw and activated sludge for removing methylene blue. *Int. J. Environ. Sci. Technol.* **2023**, *20* (2), 1673−1688.
(21) Aziz, S.; Uzair, B.; Muhammad, I. A.; Anbreen, S.; Umber, F.; Khalid, M.; Aljabali, A. A.; Mishra, Y.; et al.*et al.* Synthesis and characterization of nanobiochar from rice husk biochar for the removal of safranin and malachite green from water. *Environ. Res.* **2023**, *238*, No. 116909.
(22) Wu, J.; Yang, J. W.; Huang, G. H.; Xu, C. H.; Lin, B. F. Hydrothermal carbonization synthesis of cassava slag biochar with excellent adsorption performance for Rhodamine B. *J. Cleaner Prod.* **2020**, *251*, No. 119717.
(23) Wei, M.; Marrakchi, F.; Yuan, C.; Chen, X. X.; Jiang, D.; Zafar, F. F.; Fu, Y. X.; Wang, S. Adsorption modeling, thermodynamics, and DFT simulation of tetracycline onto mesoporous and high-surface-area NaOH-activated macroalgae carbon. *J. Hazard. Mater.* **2022**, *425*, No. 127887.
(24) Hou, Z. Q.; Tao, Y. P.; Bai, T. C.; Liang, Y.; Huang, S. R.; Cai, J. J. Efficient Rhod-amine B removal by N-doped hierarchical carbons obtained from KOH activation and urea oxidation of glucose hydrochar. *J. Environ. Chem. Eng.* **2021**, *9*, No. 105757.
(25) Li, X.; Li, R.; He, D.; Feng, X. Superior Adsorption Performance of TiO2-Loaded Chitosan Biochar for Rhodamine B Dye. *Russ. J. Inorg. Chem.* **2023**, *68*, 084−1095.
(26) Kim, D.-Y.; Jung, G. Effects of Pyrolysis and Ball-Milling on the Physicochemical and Rhodamine B Removal Characteristics of Rice-Bran-Derived Biochar. *Appl. Sci.* **2023**, *13*, No. 4288.
(27) Somsiripan, T.; Sangwichien, C. Enhancement of adsorption capacity of Methylene blue, Malachite green, and Rhodamine B onto KOH activated carbon derived from oil palm empty fruit bunches. *Arab. J. Chem.* **2023**, *16*, No. 105270.
(28) Wu, T.; Yang, G.; Cao, J.; Xu, Z.; Jiang, X. Activation and adsorption mechanisms of methylene blue removal by porous biochar adsorbent derived from eggshell membrane. *Chem. Eng. Res. Des.* **2022**, *188*, 330−341.
(29) Paluch, D.; Bazan-Wozniak, A.; Nosal-Wierci′nska, A.; Cielecka-Piontek, J.; Pietrzak, R. Fennel Seed Biochar: A Sustainable Approach for Methylene Blue Removal from Aqueous Solutions. *Materials* **2024**, *17*, No. 4350.
(30) Guo, S. J.; Zou, Z. Y.; Chen, Y.; Long, X. X.; Liu, M.; Li, X. P.; Tan, J. H.; Chen, R. Z. Synergistic effect of hydrogen bonding and π-π interaction for enhanced adsorption of rhodamine B from water using corn straw biochar. *Environ. Pollut.* **2023**, *320*, No. 121060.
(31) Su, Y.; Zheng, Y.; Feng, M.; Chen, S. Magnetic Luffa-Leaf-Derived Hierarchical Porous Biochar for Efficient Removal of Rhodamine B and Tetracycline Hydrochloride. *Int. J. Mol. Sci.* **2022**, *23* (24), No. 15703.
(32) Zhang, H.; Peng, B.; Liu, Q.; Wu, C.; Li, Z. Preparation of porous biochar from heavy bio-oil for adsorption of methylene blue in wastewater. *Fuel Process. Technol.* **2022**, *238*, No. 107485.
(33) Patra, B. R.; Nanda, S.; Dalai, A. K.; Meda, V. Taguchi-based process optimization for activation of agro-food waste biochar and performance test for dye adsorption. *Chemosphere* **2021**, *285*, No. 131531.
(34) Agassin, S. T. R.; Dognini, J.; Paulino, A. T. Raw Rice Husk Biochar as a Potential Valuable Industrial Byproduct for the Removal of Rhodamine B from Water. *Water* **2023**, *15*, No. 3849.
(35) Hua, Z. X.; Pan, Y. P.; Hong, Q. K. Adsorption of Congo red dye in water by orange peel biochar modified with CTAB. *RSC Adv.* **2023**, *13*, 12502−12508.
(36) Abdulkareem, A. S.; Hamzat, W. A.; Tijani, J. O.; Egbosiuba, T. C.; Mustapha, S.; Abubakre, O. K.; Okafor, O. K.; Babayemi, A. K. Isotherm, kinetics, thermodynamics and mechanism of metal ions adsorption from electroplating wastewater using treated and functionalized carbon nanotubes. *J. Environ. Chem. Eng.* **2023**, *11* (1), No. 109180.
(37) Li, K.; Wu, J.; Li, X.; Li, B.; Zhou, D. Preparation of porous composite hydrogel with ultra-high dye adsorption capacity based on biochar: Adsorption behaviors and mechanisms. *Chem. Eng. Sci.* **2024**, *295*, No. 120115.

https://doi.org/10.1021/acsomega.5c00307
ACS Omega 2025, 10, 18753−18763